




# Nanoscale phase separations in as-fabricated thick super duplex stainless steels

Vahid A. Hosseini<sup>1,\*</sup> , Kristina Lindgren<sup>2</sup>, Mattias Thuvander<sup>2</sup>, Daniel Gonzalez<sup>3</sup>, James Oliver<sup>4</sup>, and Leif Karlsson<sup>1</sup>

<sup>1</sup>Department of Engineering Science, University West, 461 86 Trollhättan, Sweden

<sup>2</sup>Department of Physics, Chalmers University of Technology, 412 96 Gothenburg, Sweden

<sup>3</sup>Bodycote, 735 23 Surahammar, Sweden

<sup>4</sup>Outokumpu Stainless AB, 774 41 Avesta, Sweden

Received: 24 November 2020

Accepted: 29 March 2021

Published online:  
19 April 2021

© The Author(s) 2021

## ABSTRACT

Nanoscale phase separations, and effects of these, were studied for thick super duplex stainless steel products by atom probe tomography and mechanical testing. Although nanoscale phase separations typically occur during long-time service at intermediate temperatures (300–500 °C, our results show that slowly cooled products start to develop Fe and Cr separation and/or precipitation of Cu-rich particles already during fabrication. Copper significantly slowed down the kinetics at the expense of Cu-rich particle precipitation, where the high-copper material subjected to hot isostatic pressing (HIP), with  $\Delta t_{500-400}$  of 160 s and the low-copper hot-rolled plate with  $\Delta t_{500-400}$  of 2 s had the same level of Fe and Cr separation. The phase separations resulted in lower toughness and higher hardness of the HIP material than for hot-rolled plate. Therefore, both local cooling rate dependent and alloy composition governed variations of phase separations can be expected in as-fabricated condition.

## Introduction

Duplex stainless steels (DSSs), with a balanced fraction of ferrite and austenite, provide a great combination of superior mechanical properties and corrosion resistance. Super duplex stainless steels (SDSSs), containing a higher content of Cr, Mo, N, and Ni compared to standard grades, provide even higher corrosion resistance and better mechanical

properties [1–3]. Phase separation in the ferrite may, however, occur during intermediate temperature applications by the formation of alpha ( $\alpha$ )-alpha prime ( $\alpha'$ ) domains, Cu-rich particles (CRPs), G-phase particles, etc., causing a toughness loss, known as “475 °C-embrittlement”. The separation occurs on a nanoscale in the temperature range of about 300–500 °C [4–8]. The  $\alpha$ - $\alpha'$  separation during quenching and different solutionizing treatments has

Handling Editor: Sophie Primig.

Address correspondence to E-mail: Vahid.hosseini@hv.se

<https://doi.org/10.1007/s10853-021-06056-0>

been the subject of different studies. In two studies [9, 10], the degree of this phase separation has been calculated theoretically. Both showed that spinodal decomposition can occur during quenching but that, depending on the composition, it might be avoided by faster cooling. Zhou et al. [11] showed that Cr atoms clustered in the solutionized condition of a Fe-46.6%Cr alloy, where this clustering decreased with increasing solutionizing temperature. Xu et al. [12] also studied binary Fe-(20–40)% Cr alloys in furnace-cooled and brine-quenched conditions and showed that the initial state of phase separation may have a significant effect on the outcome of subsequent aging. Lemoine et al. [13] also mentioned the progression of spinodal decomposition during quenching of a cast DSS alloy. Some recent studies also showed that noticeable phase separation can occur already after 3 min aging in SDSSs, with material datasheets indicating up to 50% toughness loss [4, 14]. It, therefore, raises the concern of what the level of this phase separation is in as-fabricated thick SDSS sections and how it impacts the properties. Particularly, in previous studies of hot isostatically pressed (HIPed SDSS products, Smuk et al. [15, 16] reported a toughness loss during cooling; however, its main cause remained unrevealed.

The aim of the present study is to investigate the state of phase separations in industrially fabricated thick SDSS plates and copper-bearing HIPed SDSS products using atom probe tomography (APT), arc heat treatment, scanning electron microscopy, and thermodynamic calculations. Low-temperature impact toughness and microhardness tests were employed to study how detrimental these phase separations are for the mechanical properties. The paper also shows the complex effect of Cu on phase separations.

## Experimental

### Materials

SDSS samples were extracted from as-fabricated hot-rolled and HIPed steels. The chemical composition, designation of samples, and cooling time from 500 to 400 °C ( $\Delta t_{400-500}$ ) are detailed in Table 1 and 2. The cooling time was provided by the materials' fabricators for their specific processing conditions. The samples, in the shape of thin plates, were produced

from the center and surface of the 33-mm-thick plate, respectively.

### Microscopy and mechanical testing

Optical microscopy was performed to measure the ferrite and austenite fractions. The samples were prepared with a standard metallography procedure followed by etching with Beraha, and the microstructure was analyzed with a Zeiss Axio Imager.M2m optical microscope, and the average of at least 5 fields was measured using ImagePro software to report the austenite fraction. A Zeiss Gemini 3 scanning electron microscope equipped with energy-dispersive X-ray spectroscopy (EDS) was used to measure the chemical composition of the ferrite. The average of 4 fields for CuHIP400s and 7 fields for CuHIP160s was calculated to measure chemical composition, as shown in Fig. 1.

The microhardness of ferrite and austenite was measured with 0.01 N force using Shimadzu HMV-2. The microhardness was measured for 10 points at room temperature. For plate, we measured on both TD and ND surfaces. The Charpy impact toughness test was carried out at  $-40$  °C using a Zwick Roll machine. The sample size was 55 mm  $\times$  10 mm  $\times$  5 mm, and three samples were tested for each condition.

### Atom probe tomography

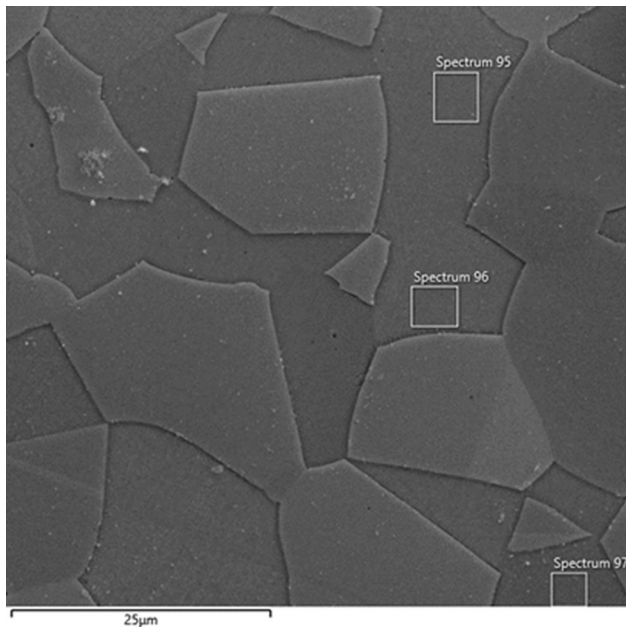
The APT analysis was employed to investigate the level of phase separation in the plate and copper-bearing HIP (CuHIP) samples. Initially, 15 mm  $\times$  0.3 mm  $\times$  0.3 mm samples were produced by cutting. Then, the samples were electropolished by 10% perchloric acid and 19 V as the coarse polishing step followed by 2% perchloric acid and 19 V as the fine polishing step, both steps at room temperature. A local electrode atom probe, LEAP 3000X HR<sup>TM</sup>, equipped with a reflectron for improved mass resolution was used. The analysis was done at 55 K with a 20% voltage pulse fraction, a pulse frequency of 200 kHz, and an evaporation rate of 0.2%. The APT data was reconstructed using IVAS 3.4/3.6, with a field of 33 V/nm, a geometric field factor ( $k$ ) of 4.0, and an image compression factor of 1.65. The radial distribution functions (RDFs) were used to analyze the extent of the spinodal decomposition following the method described by Zhou et al. [17]. Cu particles

**Table 1** Chemical composition of samples reported by fabricators

Sample	C (wt%)	Si (wt%)	Mn (wt%)	Cr (wt%)	Ni (wt%)	Mo (wt%)	Cu (wt%)	N (wt%)	W (wt%)
Plate Outokumpu	0.02	0.3	0.7	25.0	6.9	3.8	0.2	0.28	0.05
HIP Bodycote	0.030 max	1.00 max	1.50 max	24.0–27.0	4.5–7.0	2.9–3.9	1.5–2.5	0.25–0.30	–

**Table 2** Annealing temperature,  $\Delta t_{400-500}$  after annealing, and designation of samples

Sample	Solution annealing temperature (°C)	$\Delta t_{500-400}$ (s)	Designation
Plate—center	1100	~ 20	PlateC20s
Plate—surface	1100	~ 2	PlateS2s
HIP-condition 1	1070	~ 160	CuHIP160s
HIP-condition 2	1070	~ 400	CuHIP400s

**Figure 1** Example of areas used for measurement of ferrite chemical composition with EDS in CuHIP160s.

were removed from the analysis before the evaluation of the spinodal decomposition to not affect the results.

### Thermodynamic calculations

Thermodynamic calculations were performed using the Thermo-Calc TCFE10 software package. The equilibrium phase fractions for the plate and CuHIP compositions (the average of nominal composition) were calculated. To have a reasonable estimation of different phases, gas, chi, sigma, Laves, P1-A13, ETA,

and Mu were set as dormant, making it possible to have  $\alpha'$  as a stable phase.

### Arc heat treatment

To monitor the kinetics of spinodal decomposition on a larger scale, we used a recently developed technique called arc heat treatment, where the etching response of the spinodally decomposed area is weaker than for untransformed regions. In this method, a stationary tungsten inert gas arc was applied on a stationary disc with a diameter of 50 mm and a thickness of 6 mm mounted on a water-cooled chamber. This condition created a steady-state heat transfer condition, for 5 and 10 min on CuHIP160s and PlateS2s samples. Then, the cross section of the sample was etched with 10% NaOH with a voltage of 2 V for 10 s. As different locations have different etching responses due to different steady state temperatures, the location with spinodal decomposition showed a very light etching response due to the changing electrochemistry behavior of ferrite. More details about this novel technique are presented in Refs. [18–21].

## Results

### Thermodynamic calculations

The equilibrium phase fraction diagrams with the plate and HIPed compositions are shown in Fig. 2. The main difference between the diagrams is that CRP is stable below 896 °C for the CuHIP composition, but only below 475 °C for the plate composition,

due to higher copper in CuHIP. The equilibrium phase fraction diagrams of these two alloys between 400 and 600 °C are shown in Fig. 2. The predicted fraction of  $\alpha'$  is similar in CuHIP and the plate, as seen in Fig. 2a. The equilibrium fraction of CRP is much higher in CuHIP than for the plate, as expected in Fig. 2b. The equilibrium fractions of nitrides and R-phase are higher in CuHIP than in the plate (Fig. 2b).

### Microstructure

The microstructures of different samples are shown in Fig. 3. The plate has elongated grains oriented in the rolling direction, with a bimodal distribution of austenite grains (Fig. 3a and b). Some traces of intermetallics were also found in the center with local segregation bands occurring in thick DSS plates, as illustrated in Fig. 4. No intermetallic phases were observed in PlateS2s. The surface region has a smaller austenite spacing and a lower fraction of austenite compared to in the center (Fig. 5). The microstructure of HIPed samples reveals equiaxed grains, and the CuHIP400s has a higher austenite fraction. Therefore, the highest austenite fractions belong to the slowly cooled plate and HIP samples. The difference between the austenite fractions of two plate samples was lower than those of CuHIP samples.

### Atom probe tomography

The chemical compositions of the ferrite of the four samples were measured by APT, as detailed in Table 3. In CuHIP400s, two needles had a chemical

composition that did not agree with CuHIP160s and the equilibrium content at 1130 °C. To quantify the ferrite composition, EDS analysis was also performed on the HIPed samples. Interestingly, it was seen that the Cu contents measured with EDS of CuHIP160s and CuHIP400s were very similar. Therefore, local low-copper locations (L1) and high-copper locations (L2) appear to have formed in the CuHIP400s.

Cr–Cr RDF curves for the as-fabricated samples are shown in Fig. 6. CuHIP400s L1 showed a much more developed Cr and Fe separation compared to the other samples in this study, as shown in Fig. 6b. This separation was high enough to be seen in high Cr and high Fe isosurfaces, shown in Fig. 7. However, CuHIP400s L2 did not show any significant Cr and Fe separation. A noticeable difference in amplitude and extent of separation in the center and surface of the plate was found.

Although Cu had a positive effect by slowing down the Fe and Cr decomposition, CRPs were observed in CuHIP, as shown in Fig. 8. In the CuHIP400s, two regions with high Cu and low Cu had significantly different CRP precipitation behavior. CuHIP400s L1 showed very fine precipitates, whereas CuHIP400s L2 contained one large CRP. In CuHIP160s, the particles are smaller than in CuHIP400s L2 but much bigger than in CuHIP400s L1.

### Scanning electron microscopy

As CuHIP400s showed two distinctive particle distributions in two needles, while EDS analysis shows no specific segregation; a SEM micrograph of the

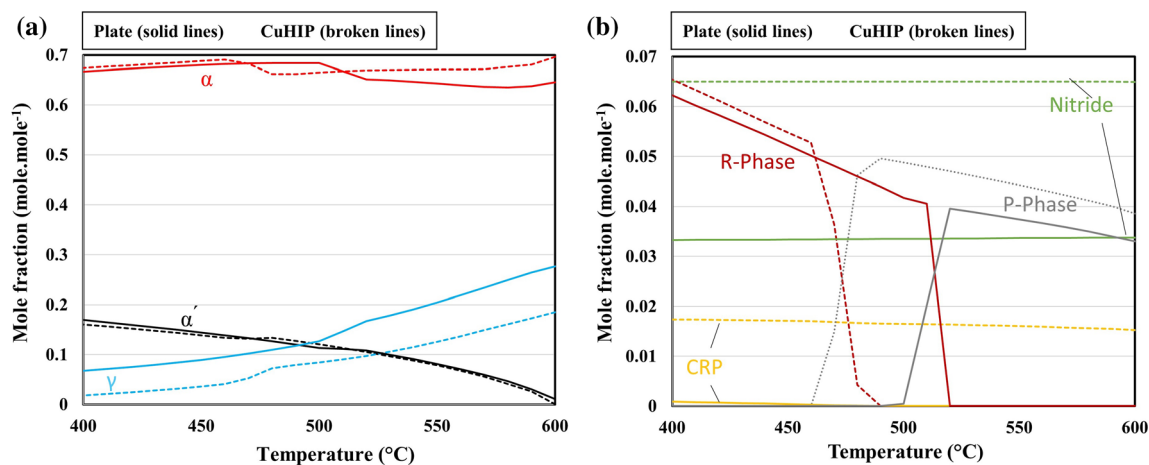


**Figure 2** Equilibrium phase diagram calculated with Thermo-Calc between 600 and 1000 °C. **a** Major phases, and **b** minor phases.

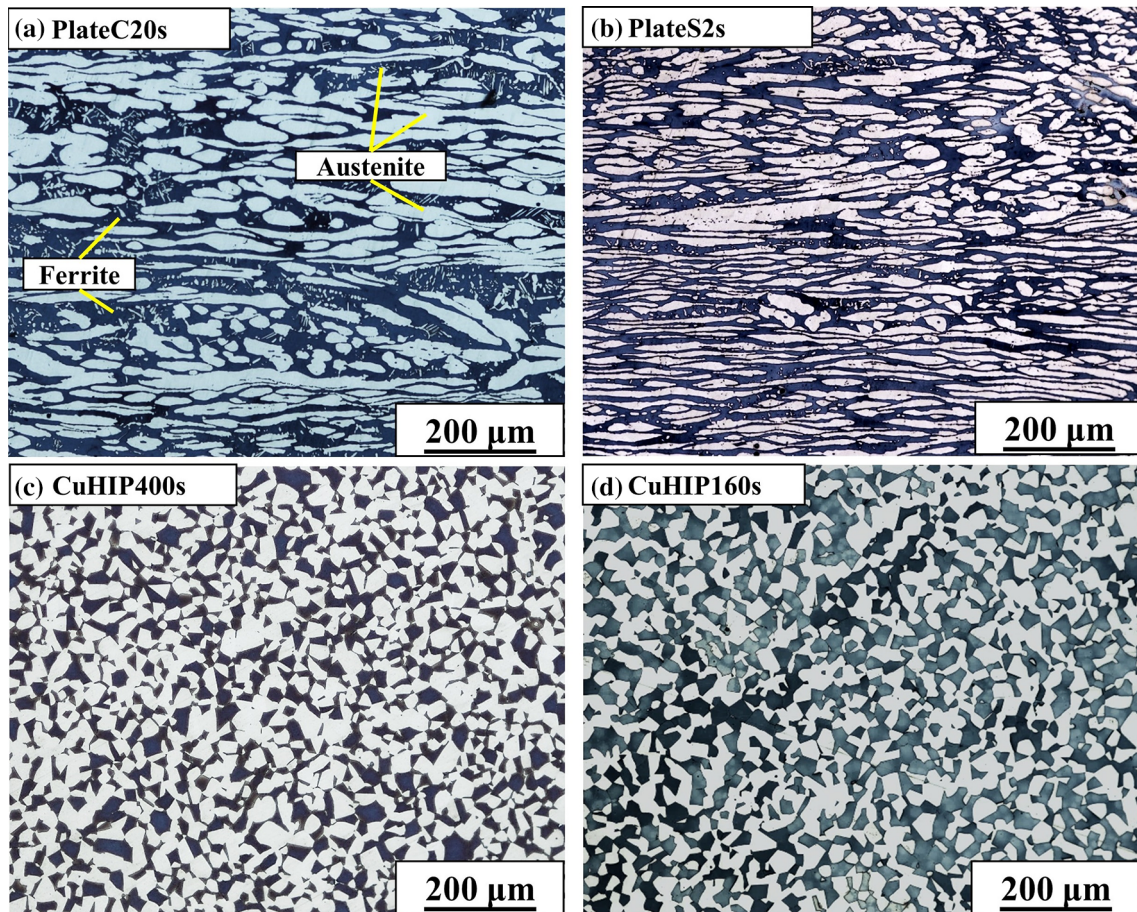


**Figure 3** Microstructure of **a** PlateC20s containing coarse austenite grains with some fine intragranular austenite, **b** PlateS2s with fine austenite grains. **c** Microstructure of

CuHIP400s, and **d** CuHIP160s. In all images, austenite is the bright-etching, and ferrite is the dark-etching phase.

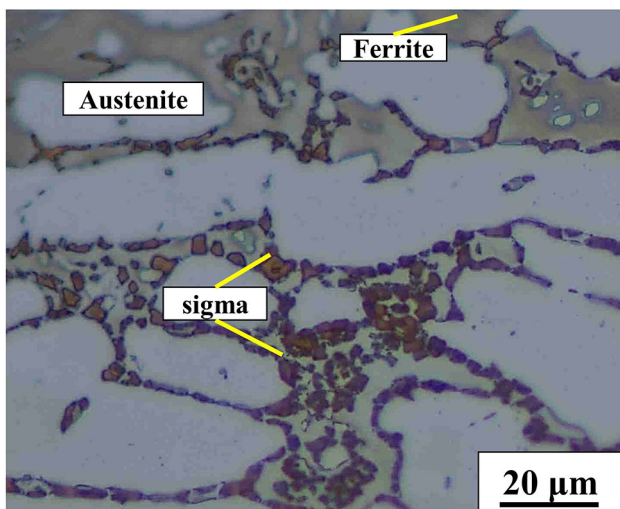


**Figure 4** Local formation of intermetallic phases due to centerline segregation of alloying elements in PlateC20s.

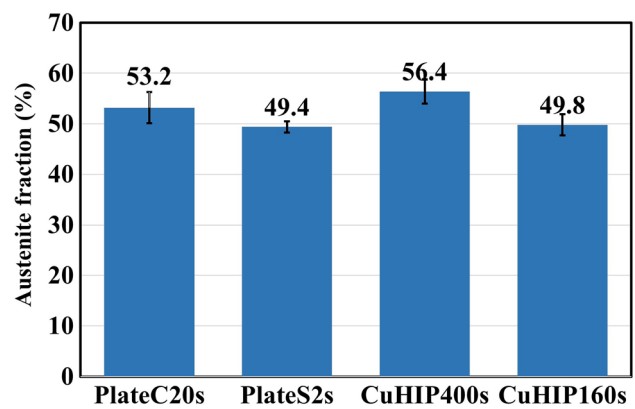


**Figure 5** Austenite fractions of different samples. The faster cooled HIP and plate samples have lower austenite fractions.

**Table 3** Chemical composition of ferrite measured by APT for all samples and EDS for HIPed samples

Element (at%)	PlateS2s	PlateC20s	CuHIP160s		CuHIP400s		
	APT	APT	APT	EDS	APT-L1	APT-L2	EDS
Cr	28.0	27.8	28.9	30.4 ± 0.2	27.9	27.8	31.0 ± 0.2
Ni	4.5	4.4	5.0	4.7 ± 0.1	5.0	4.8	3.8 ± 0.7
Mo	3.2	3.4	2.1	2.1 ± 0.1	2.3	2.6	2.2 ± 0.1
Si	0.9	0.9	1.2	1.3 ± 0.1	1.1	1.1	1.0 ± 0.1
Mn	0.6	0.6	0.5	0.8 ± 0.1	0.5	0.5	1.2 ± 0.7
Cu	0.1	0.1	1.1	1.2 ± 0.1	0.5	2.1	1.1 ± 0.2
Fe + minor elements*	Bal.	Bal.	Bal.	Bal.	Bal.	Bal.	Bal.

\*C is below 0.02 at% and P below 0.1 at%

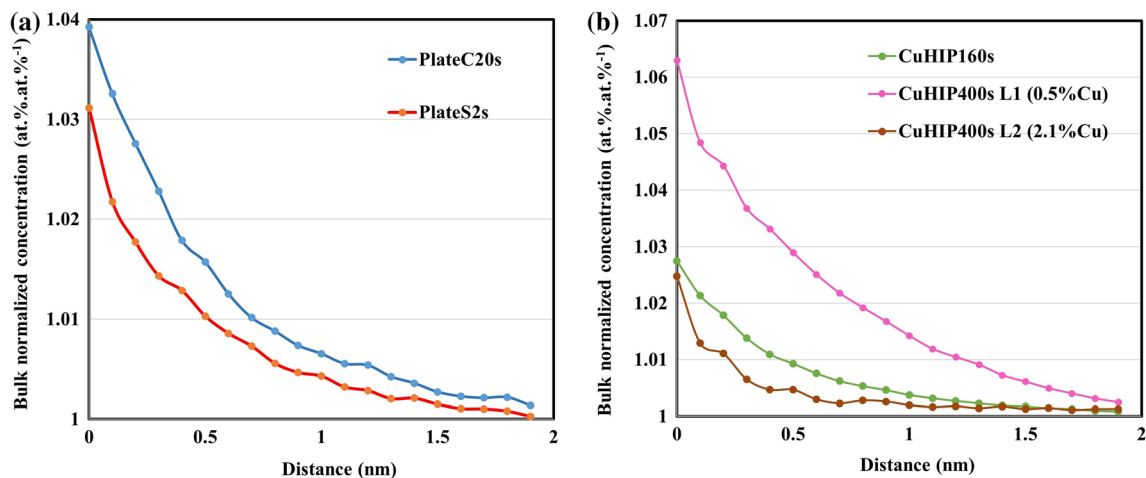


**Figure 6** **a** Cr–Cr RDF of the plate samples, **b** Cr–Cr RDF of the HIPed samples.

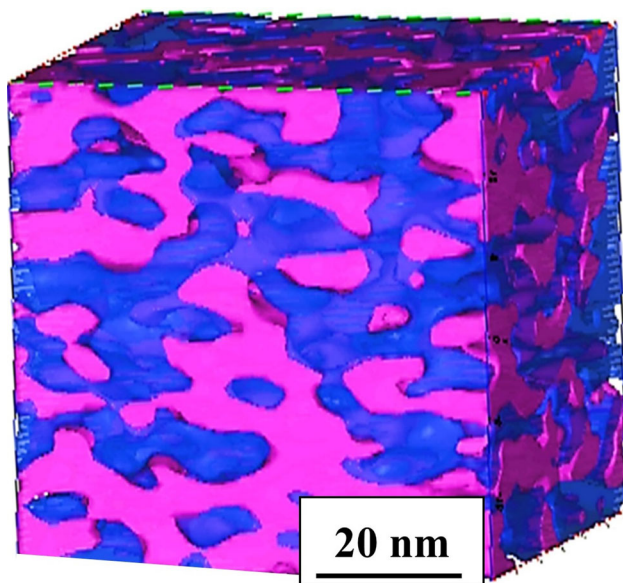


**Figure 7** High Cr (blue) and high Fe (purple) domain isosurfaces for CuHIP400s L1 showing well-developed separation. The isosurfaces are 29% Cr and 61% Fe.

sample is shown in Fig. 9. As can be seen, many relatively large Cu particles, like the one in the APT analysis CuHIP400s-L2, form with an approximate distance of 100–200 nm.

### Mechanical properties

The Charpy impact toughness of the different samples and their microhardness values of ferrite and austenite are detailed in Fig. 10, and the impact toughness values are shown in Table 4. In the plate sample, the microhardness of ferrite is slightly higher in the center, but for austenite, it is lower. The toughness of the plate samples was almost equal, which was much higher than for the HIPed samples. CuHIP400s showed the highest hardness in ferrite and the lowest toughness among all samples. Compared to CuHIP160s, its toughness was 23 J lower.

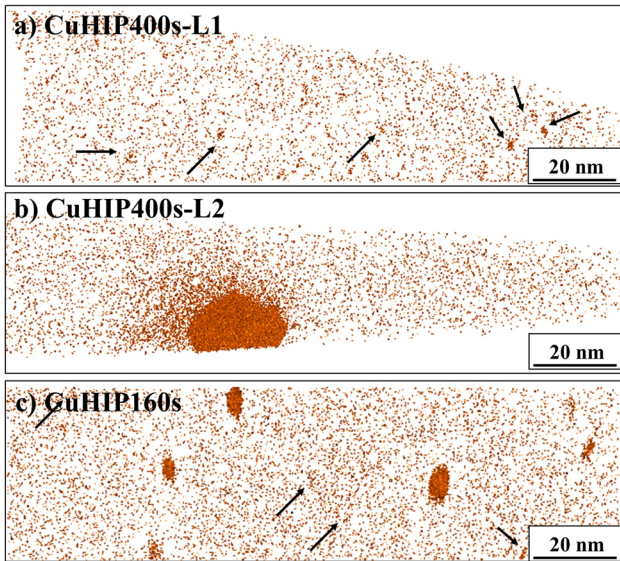


**Figure 8** Reconstruction of Cu atom positions from APT analyses for a volume with dimensions of 160 nm × 45 nm × 6 nm. The precipitation of CRPs in **a** CuHIP400s (L1: 0.5 at% Cu), arrows show the CRP clusters **b** CuHIP400s (L2: 2.1 at% Cu) **c** CuHIP160s (1.1 at% Cu).

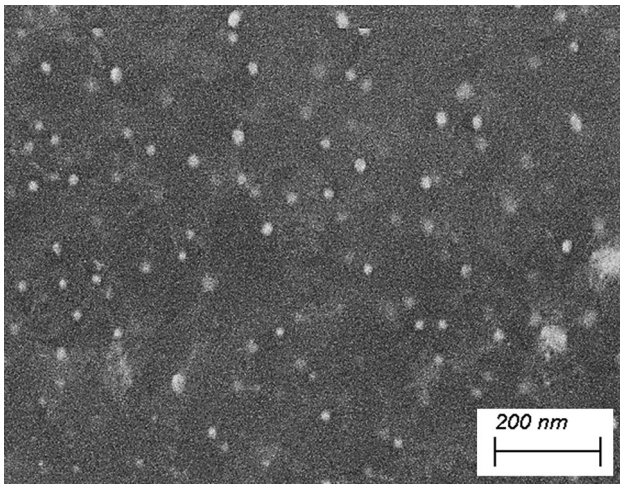


**Figure 9** SEM micrograph of CuHIP400s with large Cu particles, also seen in APT of CuHIP400s.

**Arc heat treatment**

To understand the kinetics of spinodal decomposition in the two samples CuHIP160s and Plate2s with the same initial phase separation but with different Cu contents, the cross sections of arc heat treated samples after 2 and 10 min were studied, as shown in Fig. 11. In the previous studies [18–21], it was illustrated that at an isotherm line of 475 °C in the arc heat treated samples, a low etching contrast is seen due to

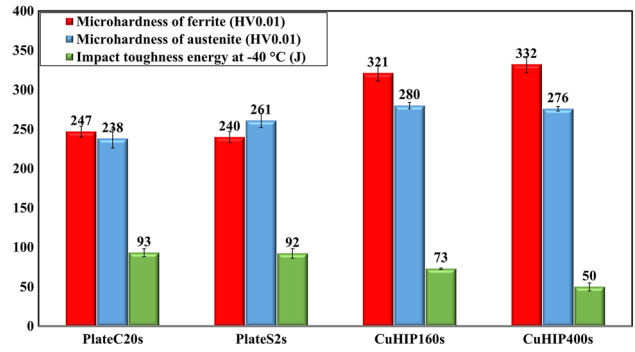


**Figure 10** Microhardness and impact toughness of the as-fabricated CuHIP and Plate SDSS.

**Table 4** The values of three impact toughness measurements

Sample	Impact toughness energy at – 40 °C (J)
PlateC20s	97, 96, 88
PlateS2s	85, 94, 96
CuHIP160s	72, 72, 73
CuHIP400s	44, 51, 53

the progress of spinodal decomposition, supported by hardness testing and APT analysis. In the current study, CuHIP160s did not show any low contrast etching around 475 °C isotherms after 5 min arc heat treatment, while this was seen after 10 min. In contrast, PlateS2s showed indications of spinodal decomposition already after 20 s, which became very visible after 5 min arc heat treatment.

**Discussion**

Phase balance and grain morphology have an impact on the final properties of DSS [22]. The austenite grain morphology in the plate and HIPed samples are dictated by the processing. In the hot-rolled plates, the stresses and strains are anisotropic during fabrication, causing the elongated austenite grains in the rolling direction. In contrast, isostatic pressure during HIP results in the formation of equiaxed austenite grains. The higher austenite fraction in the center of plates and in CuHIP400s is the result of the slower cooling after solutionizing (Fig. 5). However, all four conditions meet the required austenite fraction for DSS [23, 24].

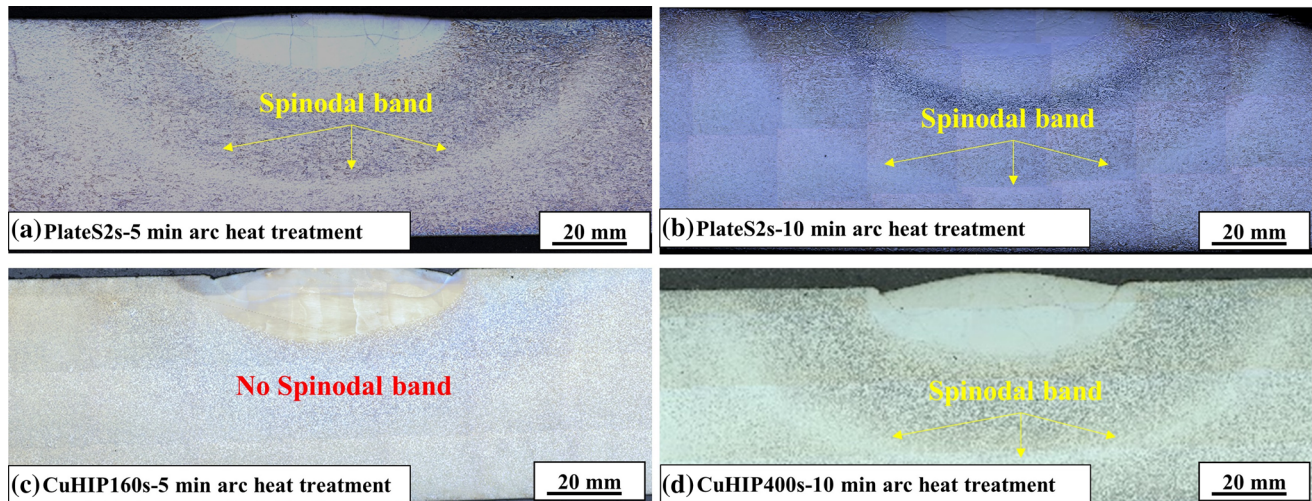


**Figure 11** Cross section of arc heat treated samples for 5 and 10 min. **a** 5 min arc heat treated PlateS **b** 10 min arc heat treated PlateS **c** 5 min arc heat treated CuHIP160s **d** 10 min arc heat treated CuHIP160s. No trace of 475 °C etching response in

CuHIP160s after 5 min arc heat treatment. Different etching response at 475 °C after 10 min heat treatment in CuHIP160s and after 5 and 10 min in PlateS2s.

### Phase separations

In addition to the phase balance and grain morphology, phase separations on the nanoscale level can significantly degrade the performance of DSS. In this study, Cr and Fe separation and/or CRP precipitation were detected in the alloys. Cr and Fe separation, at the early stages, is challenging to characterize. However, RDF analysis of the APT data is a reliable approach that statistically shows the tendency of Cr atoms to attract each other [17]. In the plate sample, the quenching rate is clearly affecting the phase separation level. The comparison of the present RDF results with data from literature is illustrated in Fig. 12. The unaged 6-mm plate [25] has a higher RDF than the PlateS20s and CuHIP160s. Pettersson et al. [25] did not find a noticeable change after 3000 h aging at 300 °C. The PlateC20s showed slightly larger and wider Cr–Cr separations than for the aged condition reported in the literature [25, 26], meaning that the level of initial separation during slower cooling such as in the center of the plate might be higher than that in aged conditions.

### Cu effects

Cu influenced the level of Cr and Fe separation as seen by comparing CuHIP400s L1 with L2 and CuHIP160s with PlateS2s. The difference between CuHIP400s L1 and L2 is 1.5. at% higher Cu content in

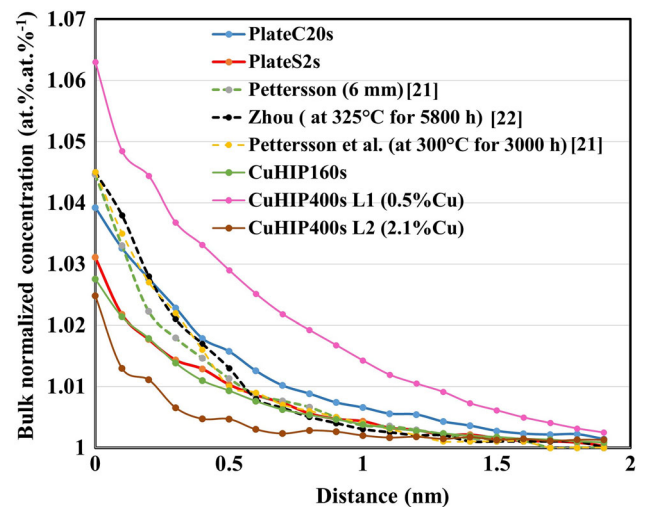


**Figure 12** Comparison of Cr–Cr RDFs of samples in this study and literature.

L2 than in L1, including CRPs in the composition. CuHIP400s L2 had the lowest level of Cr and Fe separation compared to the other samples in this study and results reported in the literature [25, 26]. The other comparison that verifies the importance of Cu is between CuHIP160s and PlateS2s. Their RDFs were almost identical, but the PlateS2s was cooled down significantly faster than CuHIP160s. The main difference between their composition is 1 at% higher Cu and 1 at% lower Mo in the CuHIP160s ferrite than in the PlateS20s ferrite. Li et al. [27] reported that Mo does not have a significant effect on spinodal



decomposition. Hedström et al. [28] did not find any phase separation in Cu-containing Fe-20Cr after 10 h heat treatment. Both studies, however, were for longer aging times. Our results show that Cu is a key element slowing down the spinodal decomposition in SDSS during fabrication. Arc heat treatment results also revealed that PlateS2s had faster spinodal decomposition during aging than CuHIP160s, supporting that Cu slows down the spinodal decomposition kinetics.

In addition to Cr and Fe separation, CRPs also precipitated during cooling in the HIPed samples. This is in line with Thermo-Calc calculations showing that CRPs are expected to form with higher fractions and at higher temperatures in HIPed samples. We expect that low-copper regions form because of Cu depletion in the matrix caused by precipitation of large CRPs, as shown in the SEM micrograph, at higher temperatures during cooling. Then during further cooling at lower temperatures, there is secondary precipitation due to the significant reduction in Cu solubility. Therefore, two different regions were formed, which is observed in CuHIP400s. In CuHIP160s, the smaller CRPs were quite similar to Cu clusters reported by Thuvander et al. [6] after aging for 5800 h at 325 °C of low-copper SDSS (0.3 wt%). Further studies of CRPs are needed to fully understand the distribution and precipitation behavior.

### Influence on properties

Understanding the impact of these local phase separations on the mechanical properties is challenging as ferrite, austenite, and their morphology and interaction with each other influence the final properties. Fast cooling after annealing can create residual stresses close to the surface, resulting in higher hardness. The center had more time to cool down and accommodate the stresses. The higher hardness of ferrite in the center, despite less residual stresses, is, therefore, most probably the result of a higher degree of phase separation. Interestingly, the impact toughness of both plate samples showed quite similar results. At the surface, the lower austenite content and possibly more residual stress during the fast cooling of the surface have negative effects on the toughness, but the absence of secondary phases and less phase separation have positive effects. In the center, some sigma phase precipitation and a slightly

higher level of spinodal decomposition have negative effects on the toughness, but higher austenite content and lower residual stresses have a positive effect. Therefore, they show similar toughness levels while having different thermomechanical histories and microstructures.

Comparing the PlateS2s and CuHIP160s, with the same level of spinodal decomposition but different Cu content may indicate that the presence of CRPs is responsible for the higher hardness of ferrite and lower toughness in CuHIP160s. Comparing mechanical properties of CuHIP400s and CuHIP160s shows that larger CRPs coupled with Cr and Fe decomposed regions resulted in higher hardness and lower impact toughness in CuHIP400s sample even with a higher austenite content (Fig. 5).

This study showed that in industrial hot-rolled and HIPed alloys, nanoscale phase separations can occur during fabrication, which can influence the mechanical properties. The reason for low impact toughness in Cu containing HIPed SDSS after simulated industrial cooling conditions remained unexplained in previous studies [15, 16]. However, our results show that well-developed Cr and Fe separations and CRPs are the main causes of this reduction. Zhou et al. [29, 30] calculated that a larger initial Fe and Cr phase separation during cooling of Fe-45% Cr may be a dominant factor impacting the level of phase separation during service. Our experimental results confirmed a noticeable level of phase separation in the as-fabricated condition. An important question is whether this phase separation has the same impact on properties as aging at 475 °C or not. Further studies are needed to investigate how these nanoscale phase separations evolve at intermediate temperatures.

### Conclusions

In this paper, nanoscale phase separations were studied for thick as-fabricated hot-rolled plates and HIPed SDSS products. Phase separation was observed for Fe and Cr in slowly cooled material. Alloying with copper significantly reduced the Cr and Fe separation at the expense of CRP precipitation, where CuHIP160s and PlateS2s had the same level of Fe and Cr separation but significantly different cooling rates. CRP precipitation resulted in lower impact toughness in HIPed material compared

to the rolled plate for comparable Cr and Fe separation. Locally, Cu depleted and enriched areas formed in slowly cooled HIPed material. The Cu depleted regions showed much smaller CRPs and more developed Fe and Cr phase separation compared to enriched regions. This nonuniform nanoscale structure decreased the impact toughness of slowly cooled HIP SDSS significantly compared to when cooled faster. It is concluded that nanoscale phase separation may be present in thick as-fabricated SDSS products for different fabrication routes to such an extent that it affects the mechanical properties.

## Acknowledgements

The author would like to acknowledge KK-Stiftelsen for funding of “ALWAYS project”. The help received from Nicklas Folkesson, ESAB AB, is also highly acknowledged.

## Funding

Open access funding provided by University West.

## Declarations

**Conflicts of interest** The authors declare no conflicts of interest.

**Open Access** This article is licensed under a Creative Commons Attribution 4.0 International License, which permits use, sharing, adaptation, distribution and reproduction in any medium or format, as long as you give appropriate credit to the original author(s) and the source, provide a link to the Creative Commons licence, and indicate if changes were made. The images or other third party material in this article are included in the article’s Creative Commons licence, unless indicated otherwise in a credit line to the material. If material is not included in the article’s Creative Commons licence and your intended use is not permitted by statutory regulation or exceeds the permitted use, you will need to obtain permission directly from the copyright holder. To view a copy of this licence, visit <http://creativecommons.org/licenses/by/4.0/>.

## References

- [1] Nilsson J-O, Chai G (2010) The physical metallurgy of duplex stainless steels. Paper presented at the duplex stainless steel conference, Beaune, France
- [2] Hosseini VA, Karlsson L, Örnek C, Reccagni P, Wessman S, Engelberg D (2018) Functionally graded microstructure of super duplex stainless steel. *Mater Charact* 139:390–400
- [3] Otárola T, Hollner S, Bonnefois B, Anglada M, Coudreuse L, Mateo A (2005) Embrittlement of a superduplex stainless steel in the range of 550–700 °C. *Eng Fail Anal* 12(6):930–941. <https://doi.org/10.1016/j.engfailanal.2004.12.022>
- [4] Hosseini VA, Thuvander M, Wessman S, Karlsson L (2018) Spinodal decomposition in functionally graded super duplex stainless steel and weld metal. *Metall Mater Trans A* 49(7):2803–2816
- [5] Örnek C, Burke M, Hashimoto T, Engelberg D (2017) 748 K (475° C embrittlement of duplex stainless steel: effect on microstructure and fracture behavior. *Metall Mater Trans A* 48(4):1653–1665
- [6] Thuvander M, Zhou J, Odqvist J, Hertzman S, Hedström P (2012) Observations of copper clustering in a 25Cr–7Ni super duplex stainless steel during low-temperature aging under load. *Philos Mag Lett* 92(7):336–343
- [7] Lach TG, Frazier WE, Wang J, Devaraj A, Byun TS (2020) Precipitation-site competition in duplex stainless steels: Cu clusters versus spinodal decomposition interfaces as nucleation sites during thermal aging. *Acta Mater* 196:456–469
- [8] Francis R, Byrne G (2016) The detection of alpha prime in duplex stainless steels. Paper presented at the CORROSION 2016, Vancouver, British Columbia, Canada, March 2016
- [9] Huston EL, Cahn JW, Hilliard JE (1966) Spinodal decomposition during continuous cooling. *Acta Metall* 14(9):1053–1062. [https://doi.org/10.1016/0001-6160\(66\)90193-3](https://doi.org/10.1016/0001-6160(66)90193-3)
- [10] Carmesin HO, Heermann DW, Binder K (1986) Influence of a continuous quenching procedure on the initial stages of spinodal decomposition. *Z Phys B Condens Matter* 65(1):89–102. <https://doi.org/10.1007/bf01308403>
- [11] Zhou J, Odqvist J, Ågren J, Ruban A, Thuvander M, Xiong W, Olson GB, Hedström P (2015) Direct atom probe tomography observations of concentration fluctuations in Fe–Cr solid solution. *Scr Mater* 98:13–15. <https://doi.org/10.1016/j.scriptamat.2014.10.035>
- [12] Xu X, Odqvist J, Colliander MH, King S, Thuvander M, Steuwer A, Hedström P (2017) Effect of cooling rate after solution treatment on subsequent phase separation during aging of Fe–Cr alloys: a small-angle neutron scattering

- study. *Acta Mater* 134:221–229. <https://doi.org/10.1016/j.actamat.2017.06.001>
- [13] Lemoine C, Fnidiki A, Teillet J, Hédin M, Danoix F (1998) Mossbauer study of the ferrite decomposition in unaged duplex stainless steels. *Scr Mater* 39(1):61–66
- [14] Otokumpu O (2013) Handbook of stainless steel, Avesta Resarch Centre, Avesta. Outokumpu Oyj, Sweden
- [15] Smuk O, Hänninen H, Liimatainen J (2004) Mechanical and corrosion properties of P/M-HIP super duplex stainless steel after different industrial heat treatments as used for large components. *Mater Sci Technol* 20(5):641–644
- [16] Smuk O, Nenonen P, Hänninen H, Liimatainen J (2002) Precipitation of secondary phases in duplok 27 duplex stainless steel with emphasis on copper effects, technical report, Report number: TKK-MTR-6/02, Helsinki University of Technology
- [17] Zhou J, Odqvist J, Thuvander M, Hedström P (2013) Quantitative evaluation of spinodal decomposition in Fe–Cr by atom probe tomography and radial distribution function analysis. *Microsc Microanal* 19(3):665–675
- [18] Cederberg E, Hosseini VA, Kumara C, Karlsson L (2020) Physical simulation of additively manufactured super duplex stainless steels—microstructure and properties. *Addit Manuf* 34:101269
- [19] Hosseini VA, Karlsson L, Hurtig K, Choquet I, Engelberg D, Roy MJ, Kumara C (2017) A novel arc heat treatment technique for producing graded microstructures through controlled temperature gradients. *Mater Des* 121:11–23. <https://doi.org/10.1016/j.matdes.2017.02.042>
- [20] Hosseini VA, Thuvander M, Wessman S, Karlsson L (2018) Spinodal decomposition in functionally graded super duplex stainless steel and weld metal. *Metall Mater Trans A*. <https://doi.org/10.1007/s11661-018-4600-9>
- [21] Hosseini VA, Karlsson L, Engelberg D, Wessman S (2018) Time-temperature-precipitation and property diagrams for super duplex stainless steel weld metals. *Weld World*. <https://doi.org/10.1007/s40194-018-0548-z>
- [22] Sato Y, Nelson T, Sterling C, Steel R, Pettersson C-O (2005) Microstructure and mechanical properties of friction stir welded SAF 2507 super duplex stainless steel. *Mater Sci Eng A* 397(1–2):376–384
- [23] Putz A, Althuber M, Zelić A, Westin E, Willidal T, Enzinger N (2019) Methods for the measurement of ferrite content in multipass duplex stainless steel welds. *Weld World* 63(4):1075–1086
- [24] Hosseini VA, Hurtig K, Eyzop D, Östberg A, Janerik P, Karlsson L (2018) Ferrite content measurement in super duplex stainless steel welds. Paper presented at the IIW meeting Bali
- [25] Pettersson N, Wessman S, Thuvander M, Hedström P, Odqvist J, Pettersson RF, Hertzman S (2015) Nanostructure evolution and mechanical property changes during aging of a super duplex stainless steel at 300° C. *Mater Sci Eng A* 647:241–248
- [26] Zhou J, Odqvist J, Thuvander M, Hertzman S, Hedström P (2012) Concurrent phase separation and clustering in the ferrite phase during low temperature stress aging of duplex stainless steel weldments. *Acta Mater* 60(16):5818–5827. <https://doi.org/10.1016/j.actamat.2012.07.022>
- [27] Li S, Wang Y, Wang X (2019) Influence of Mo additions on the mechanical properties of cast duplex stainless steels before and after thermal aging. *Metals* 9(3):295
- [28] Hedström P, Huyan F, Zhou J, Wessman S, Thuvander M, Odqvist J (2013) The 475° C embrittlement in Fe–20Cr and Fe–20Cr–X (X=Ni, Cu, Mn) alloys studied by mechanical testing and atom probe tomography. *Mater Sci Eng A* 574:123–129
- [29] Zhou J, Odqvist J, Höglund L, Thuvander M, Barkar T, Hedström P (2014) Initial clustering—a key factor for phase separation kinetics in Fe–Cr-based alloys. *Scr Mater* 75:62–65
- [30] Zhou J, Odqvist J, Ruban A, Thuvander M, Xiong W, Ågren J, Olson GB, Hedström P (2017) Effect of solution treatment on spinodal decomposition during aging of an Fe–46.5 at% Cr alloy. *J Mater Sci* 52(1):326–335. <https://doi.org/10.1007/s10853-016-0333-6>

**Publisher's Note** Springer Nature remains neutral with regard to jurisdictional claims in published maps and institutional affiliations.